Meteorologische Zeitschrift, Vol. **15**, No. 5, 45-56 (February 2006)

Article

Temperature and humidity profile retrievals from ground-based microwave radiometers during TUC

DOMENICO CIMINI*[1,2], TIM J. HEWISON[3], LORENZ MARTIN[4], JÜRGEN GÜLDNER[5], CATHERINE GAFFARD[3] and FRANK S. MARZANO[6]

[1]IMAA, National Research Council, Italy
[2]CIRES, University of Colorado, USA
[3]Met Office, University of Reading, United Kingdom
[4]Institute of Applied Physics, University of Bern, Switzerland
[5]Deutscher Wetterdienst, Meteorologisches Observatorium Lindenberg, Germany
[6]Center of Excellence CETEMPS, University of L'Aquila, Italy

(Manuscript received June 30, 2005; in revised form October 21, 2005; accepted November 1, 2005)

Abstract

Thermodynamic atmospheric profiles have been retrieved from ground-based microwave radiometers during the Temperature, hUmidity, and Cloud (TUC) profiling campaign. A variety of inversion methods is presented, in terms of requirements, advantages, and limitations. Results confirm the theoretical expectation that retrievals' accuracy and resolution degrade steadily with height up to 3 km, then more rapidly. At higher levels the retrievals' accuracy does not improve on that of a Numerical Weather Prediction model, which provides a background for the variational technique. Most retrieval methods produce a bias in the temperature profile above 1 km, which may be due to a bias in the absorption model used and/or observations at 51–54 GHz. Elevation scanning is shown to improve the accuracy and resolution of the retrievals in the boundary layer, but is limited by technical shortcomings.

Zusammenfassung

Thermodynamische atmosphärische Profile wurden mit bodengestützten Mikrowellenradiometern während der Temperature, hUmidity, and Cloud (TUC) profiling Kampagne gemessen. Verschiedene Inversionsmethoden werden in Bezug auf Anforderungen, Vorteile und Einschränkungen vorgestellt. Die Resultate bestätigen die theoretische Erwartung, dass die Genauigkeit und die Auflösung der gemessenen Profile kontinuierlich bis 3 km Höhe schwach und darüber stärker abnehmen. In den höheren Schichten ist die Genauigkeit der Profile nicht besser als die des numerischen Wettervorhersagemodells, das die Hintergrundfelder für das erörterte Variationsverfahren bereitstellt. Die meisten Inversionsmethoden führen zu systematischen Fehlern in den gemessenen Profilen oberhalb von 1 km, was auf systematische Fehler im verwendeten Absorptionsmodell und/oder bei der Messung der Helligkeitstemperatur zwischen 51 und 54 GHz hindeutet. Die zusätzliche Einbeziehung von Messungen unterschiedlicher Elevationswinkel verbessern die Genauigkeit und die Auflösung der abgeleiteten Profile in der planetaren Grenzschicht, wobei die Vorteile durch technische Unzulänglichkeiten eingeschränkt sind.

1 Introduction

During the period from December 2003 to February 2004, the Temperature, hUmidity, and Cloud (TUC) profiling campaign (RUFFIEUX et al., 2006) was held at the MeteoSwiss station in Payerne, Switzerland. A variety of ground-based instruments, including two microwave radiometer profilers (MWRP), joined the resident operational suite. This paper focuses on the evaluation of temperature and humidity profiles as retrieved from the measurements collected by the two MWRPs.

Ground-based microwave radiometry represents a mature technique for the retrieval of atmospheric variables such as integrated water vapour (IWV), integrated liquid water (ILW), and vertical profiles of temperature (T) and water vapour density (ρ) (WESTWATER, 1993). An important advantage is that microwave radiometers can be operated in long term unattended mode in nearly all weather conditions, with temporal resolution of the order of seconds. These features make MWRPs very appealing for planetary boundary layer research (RUFFIEUX et al., 2006), where atmospheric processes can develop in a time scale of the order of minutes. Also, MWRP measurements and products are ideal for the direct assimilation into Numerical Weather Prediction (NWP) models with the advantage of improving short-term forecast. As another application, MWRP measurements can be used as a reliable first guess in combined approaches (KLAUS et al., 2006) or ingested in integrated profiling techniques (LÖHNERT et al. 2004).

*Corresponding author: Domenico Cimini, IMAA/CNR and CU/CIRES, Tito Scalo (PZ), 85050, Italy, e-mail: cimini@imaa.cnr.it

0941-2948/2006/0099 $ 5.40
DOI: 10.1127/0941-2948/2006/0099

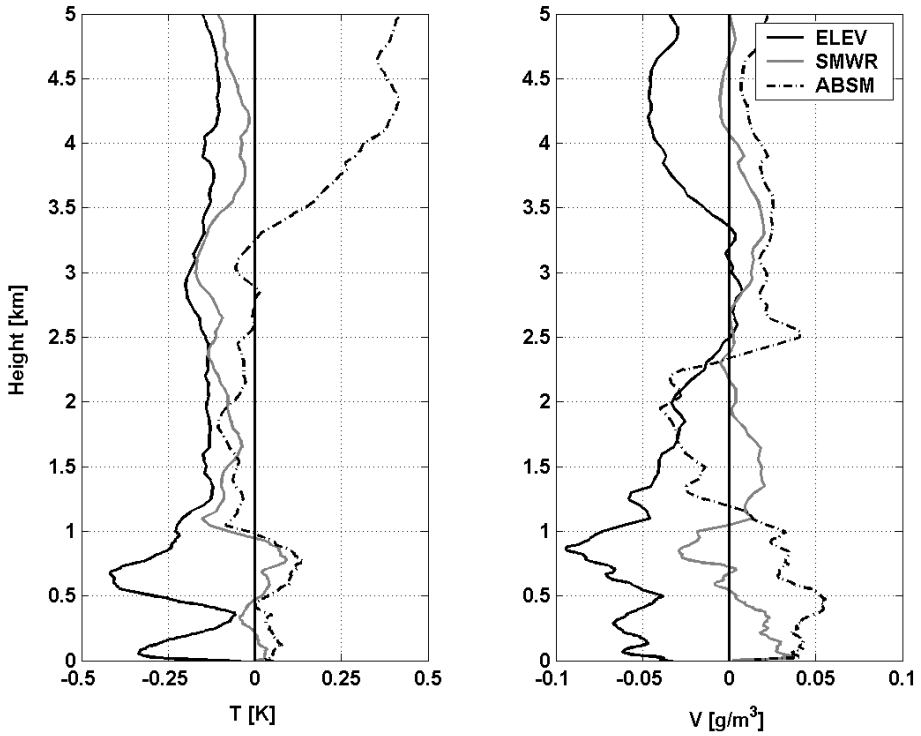

Figure 1: Simulated retrieval accuracy (rms) difference with respect to a control case when elevation scan (black solid line), additional channels (grey solid), and different absorption model (black dash-dotted) are used. Left: Temperature profiles. Right: Water vapour density profiles.

As discussed by RODGERS (2000), a variety of techniques can be used to derive atmospheric products from the measurements of thermal radiation. Each technique is based on a different approach to the inversion of the radiative tranfer equation, and thus presents its own requirements, strengths, and limitations.

This work aims to evaluate the available tools for atmospheric temperature and humidity profiling during the TUC campaign, and assess the quality of the retrievals.

2 Principles, instruments, and datasets

2.1 Basic principles

In the microwave spectral region, the principal sources of thermal radiation are atmospheric oxygen, water vapour, and liquid water within clouds. In the range between 20 and 200 GHz, emission is dominated by the oxygen complex from 50 to 70 GHz, the isolated oxygen line at 118.75 GHz, the water vapour lines at 22.235 and 183.31 GHz, and the so-called water vapour continuum arising from higher frequency lines contribution. Hydrometeors forming clouds contribute with emission, absorption, and scattering, although for lower frequencies and for non precipitating clouds, the scattering effects can be considered negligible (JANSSEN, 1993).

The intensity of radiation emitted at any altitude is proportional to the concentration of gases and hydrometeors, and to the local temperature. Thus, the principle of radiometric retrieval of temperature and humidity profiles is based on the measurement of radiation generated at different atmospheric levels. This can be accomplished in part by measuring the emitted spectrum at frequencies conveniently distributed along the wing of an absorption line/complex, which correspond to different absorption and penetration depth. For instance, temperature profiles can be estimated from spectral measurements in the 50–60 GHz band, while measurements around 22 GHz yield information on water vapour profile.

2.2 Instruments

During the TUC campaign, two MWRPs were operated at the MeteoSwiss station in Payerne, the TP/WVP-3000 and the ASMUWARA. The TP/WVP-3000 is a commercially available 12-channel MWRP built by Radiometrics Corp. Boulder, CO, USA (WARE et al., 2003), while the ASMUWARA is an unique 9-channel microwave radiometer built by the Institute of Applied Physics of University of Bern (MARTIN et al., 2006a). The TP/WVP-3000 includes a surface temperature, pressure, and humidity (TPU) sensor, while both instruments are also equipped with an infrared channel for cloud base temperature monitoring.

The microwave channels of both MWRPs are listed in Table 1. Channels in the 20–30 GHz range are valuable for IWV and ILW retrievals, but provide limited

Table 1: Nominal central frequency ($\mathbf{f_o}$), bandwidth (**B**), scanned elevation (θ) and azimuth (α) angles for TP/WVP-3000 and ASMUWARA during TUC.

TP/WVP-3000				ASMUWARA			
f_o[GHz]	B[GHz]	θ[deg]	α[deg]	f_o[GHz]	B[GHz]	θ[deg]	α[deg]
22.235	0.15	0	–	18.750	0.30	0	0
23.035	0.15	60		22.200	0.76	15	30
23.835	0.15	70		23.600	0.90	30	60
26.235	0.15	75		31.500	1.10	40	90
30.000	0.15	–75		52.500	0.59	50	120
51.250	0.15	–70		53.940	0.12	60	150
52.280	0.15	–60		55.260	0.52	70	180
53.850	0.15			57.200	1.30	75	210
54.940	0.15			151.000	4.00	80	240
56.660	0.15					85	270
57.200	0.15						300
58.800	0.15						330

profiling capability because they are highly correlated. Conversely, 50–60 GHz channels show a spectral-to-vertical mapping. In fact, opaque channels (e.g. 57.2 GHz) are mostly sensitive to the lower atmospheric levels, while more transparent channels (e.g. 52.5 GHz), are also sensitive to higher levels. The sensitivity nearly vanishes above 7 km, indicating that estimates of temperature profiles above that level rely almost uniquely on climatologic correlation with the lower troposphere. The ASMUWARA 151 GHz channel presents enhanced sensitivity to moisture and liquid water, which is useful for retrievals in dry conditions, at the expense of larger scattering contribution and higher degree of nonlinearity during humid and cloudy conditions. However, the ASMUWARA 151 GHz channel was not used for the retrievals shown in this paper, besides the simulations in Figure 1, discussed later.

2.3 TUC dataset

The TUC campaign provided about three months of radiometric measurements and retrievals under a fairly large range of environmental conditions (T from –10 to 13°C, IWV from 3 to 22 kg/m^2). As reported in Table 1, ASMUWARA repeatedly observed the atmosphere at 10 elevation and 12 azimuth angles, scanning the upper hemisphere every 15 minutes. The TP/WVP-3000 scanned 5 elevation angles every 5 minutes. Although an azimuth steering device is commercially available from the manufacturer, this was not installed on this unit. Due to malfunction of the local oscillator during the campaign, ASMUWARA channels in the oxygen band suffered of calibration difficulties that made 52.50, 53.940, and 55.260 GHz unusable (MARTIN et al., 2006a). Besides this, CIMINI et al. (2006), investigated the agreement between brightness temperature ($\mathbf{T}_b$) measured by the two MWRPs, and found agreement within the expectations in three of the four considered pairs of channels. For the remaining pair (22.2 GHz), they found about 1.7 K bias; any difference in $\mathbf{T}_b$ measurements is likely to propagate in the retrievals, so this bias must be kept in mind when comparing humidity profiles from the two instruments.

3 Retrieval techniques

A variety of techniques can be used to derive information on the atmospheric state vector **x**, from the observation vector **y**, which in our case represents radiometric and TPU measurements. In fact, the Forward (**F**) problem, represented by the Radiative Tranfer Equation (RTE), is analytically solvable and in its discrete form can be expressed by:

$$\mathbf{y} = \mathbf{F}(\mathbf{x}) \tag{3.1}$$

Conversely, because only a finite number of highly correlated observations affected by measurement error (ε) are available, the inverse problem of estimating **x** from **y**

$$\hat{\mathbf{x}} = \mathbf{R}(\mathbf{y} + \varepsilon) \tag{3.2}$$

accepts non-unique solutions and thus is said to be *ill-posed*. In this regard, the observations act as constraints that need to be coupled with auxiliary information, known *a priori*, to provide a meaningful solution. Equation 3.2 is general, and each technique is based on a different approach to the solution. In the following, we summarize the main features of the techniques applied to the radiometric observations during TUC.

3.1 Measurement-based regression

In the case an *a priori* dataset of simultaneous state vectors **x** and observations **y** is available, it is possible to solve Eq. 3.2 through empirical regression. In

the assumption of moderate non-linearity of the forward model, Eq. 3.1 can be approximated by means of first-order Taylor expansion:

$$\mathbf{y} = \mathbf{y_o} + \mathbf{K}(\mathbf{x} - \mathbf{x_o}) + \varepsilon \tag{3.3}$$

where $\mathbf{K}$ represents the Jacobian matrix ($\mathbf{K}= \delta y/\delta x$) evaluated at the expansion point $\mathbf{x_o}$. A solution for Eq. 3.2 in the linear case is given by RODGERS, (2000):

$$\hat{\mathbf{x}} = \mathbf{x_o} + (\mathbf{B^{-1}} + \mathbf{K^T E^{-1} K})^{-1} \mathbf{K^T E^{-1}} (\mathbf{y} - \mathbf{y_o}) \tag{3.4}$$

where $\mathbf{B}$ and $\mathbf{E}$ are the error covariance matrices of the state and observation vectors, and ^{T} and $^{-1}$ are the matrix transpose and inverse, respectively. This equation can be replaced by:

$$\hat{\mathbf{x}} = \mathbf{x_o} + \mathbf{C_{xy}} \mathbf{C_{yy}^{-1}} (\mathbf{y} - \mathbf{y_o}) \tag{3.5}$$

where $\mathbf{C_{xy}}$ and $\mathbf{C_{yy}}$ are extracted from the a priori data set and represent respectively the covariance matrix of the state vectors $\mathbf{x}$ and the simultaneous observations $\mathbf{y}$, and the autocovariance matrix of $\mathbf{y}$. If $\mathbf{K}$ accurately describes $\mathbf{F}$, and the statistics from the *a priori* data set well represent the covariance matrices $\mathbf{B}$ and $\mathbf{E}$, then Eq. 3.5 and Eq. 3.4 are identical. In the following we will refer to this measurement-based regression as M-REG.

3.2 Simulation-based regression

A slightly different approach with respect to the one in section 3.1 relies on the training of regression operators with a simulated, rather than measured, *a priori* dataset. This implies that a RTE solver is used to process a statistically significant set of atmospheric vectors $\mathbf{x}$ to produce synthetic observation vectors $\mathbf{y}$ and error ε that emulate the available hardware. The ensemble of atmospheric vectors $\mathbf{x}$ can be provided by historical dataset of radiosondes, when available, or by a collection of NWP outputs. This simulation-based regression will be referred to as S-REG.

3.3 Neural networks

A rather new approach for the solution of Eq. 3.2, consists in artificial Neural Networks (NN). The difference with respect to regression in sections 3.1–3.2 is basically that the operator is now a NN instead of a matrix of linear coefficients. SOLHEIM et al. (1998) carried out an analysis on inversion methods based upon synthetic data, and reported that NN outperforms other methods for retrieving water vapour and temperature profiles from radiometric data. Therefore, the software provided with the TP/WVP-3000 uses NN method. The algorithm uses standard feed forward with input, hidden, and output layers with full connection between adjacent layers. A standard back propagation algorithm is used for training, and a standard feed-forward is used for profile determination. An alternative version of the NN algorithm uses observations during elevation scans to increase the resolution in the boundary layer. We will refer to this last one as NNelev.

3.4 Optimal estimation method

Another technique for solving Eq. 3.3 is the Optimal estimation Method (OEM) (RODGERS, 2000). In this technique, an initial guess, based on *a priori* information, is given in input to Eq. 3.4 and then iterated until the solution meets a convergence criterion. Successive approximations are implemented as:

$$\begin{aligned} \hat{\mathbf{x}}_{i+1} = \mathbf{x_o} + \left(\mathbf{B^{-1}} + \mathbf{K_i^T E^{-1} K_i}\right)^{-1} \\ \mathbf{K_i^T E^{-1}} \left[(\mathbf{y} - \mathbf{F}(\hat{\mathbf{x}}_i)) + \mathbf{K}(\hat{\mathbf{x}}_i - \mathbf{x_o})\right] \end{aligned} \tag{3.6}$$

where $\hat{\mathbf{x}}_i$ and $\hat{\mathbf{x}}_{i+1}$ are the state vector at successive steps of the iteration, $\mathbf{K}_i$ and F($\hat{\mathbf{x}}_i$) are the Jacobian matrix and the forward model operator evaluated at the state vector $\hat{\mathbf{x}}$, and $\mathbf{x_o}$ is the initial guess state vector. Eq. 3.6 is applied until $\hat{\mathbf{x}}_{i+1}$ does not significantly differ from $\hat{\mathbf{x}}_i$.

3.5 One dimensional variational assimilation retrieval

One Dimensional Variational Assimilation Retrieval (1D-VAR) is an optimal estimation method used here to retrieve vertical profiles of temperature and total water to be consistent with a given set of observations, and a background field from a short-range NWP forecast. This method retrieves the state of the atmosphere that is statistically most consistent with the observations and background, given the error characteristics of each. In fact, 1D-VAR is equivalent to a Bayesian approach where the estimate is the maximum *a posteriori* probability state vector. Our implementation is similar to the *Integrated Profiling Technique* described by LÖHNERT et al. (2004). The key differences are highlighted below.

The state vector, $\mathbf{x}$, is defined as the temperature and total water on the lowest 28 levels of the Met Office mesoscale version of the Unified Model. The background information is provided by the forecast of the same model initiated 3–9 hours earlier (T+3 to T+9 forecast), interpolated to the coordinates of Payerne, valid within 30 min of the observations. This specifically excludes the influence of the radiosondes used for validation. In this study, the humidity components of the state vector are defined as the natural log of total water, ln_{qt}, where q_t is the total of the specific humidity and liquid water content. This control variable is a modified version of that suggested by DEBLONDE and ENGLISH (2003), with a smooth transfer function between water vapour for $q_t/q_{sat} < 90\%$ and liquid water for $q_t/q_{sat} > 110\%$ (where q_{sat} is the specific humidity at saturation). The

use of total water has the advantage of reducing the dimension of the state vector, enforcing an implicit supersaturation constraint and correlation between humidity and liquid water. The use of the logarithm creates error characteristics that are more closely Gaussian and prevents unphysical retrieval of negative humidity.

The Background Error Covariance, **B**, was calculated from the differences between the radiosondes and background for the whole period of TUC. This method provides a worst-case estimate of **B** as it includes contributions from the radiosondes and their representativeness errors.

The observation vector, **y**, is defined as a vector of the zenith brightness temperatures in the 12 channels of the TP/WVP-3000 microwave radiometer, plus the temperature and specific humidity measured by PTU sensors. The Observation Error Covariance, **E**, has contributions from the radiometric noise, forward model, and representativeness errors. For a discussion of these contributions, see HEWISON et al. 2006.

To speed up the calculation, a *Fast Absorption Predictor* model is used to calculate the absorption in each level below 100 hPa as a third order polynomial function of pressure, temperature and specific humidity, following LÖHNERT et al. (2004). This introduces an additional random error in the calculation of $\mathbf{T}_b$ approximately as large as the forward model error contribution. The Jacobian matrix **K** is calculated by perturbing each level of the state vector **x** by 1 K in temperature or 0.001 in ln_{qt}. **K** is only calculated for levels between the surface and 8 km, corresponding to the maximum range of likely impact from the radiometer data. For levels above this, **K**= 0. Thus, using Eq. 3.6, we adopt the following criterion to decide whether the iteration has reached convergence (RODGERS, 2000):

$$\left[\mathbf{F}(\hat{\mathbf{x}}_{i+1})-\mathbf{F}(\hat{\mathbf{x}}_i)\right]^{\mathbf{T}} \mathbf{S}_{\delta\mathbf{y}}^{-1} \left[\mathbf{F}(\hat{\mathbf{x}}_{i+1})-\mathbf{F}(\hat{\mathbf{x}}_i)\right] << d \quad (3.7)$$

where d is the dimension of **y**, and $\mathbf{S}_{\delta\mathbf{y}}$ is the covariance matrix between **y** and $\mathbf{F}(\hat{\mathbf{x}}_\mathbf{i})$. Upon convergence the retrieved state vector,$\hat{\mathbf{x}}$, is tested for statistical consistency with $\mathbf{x_o}$ and **B** by calculating the χ^2 value:

$$\chi^2 = (\hat{\mathbf{x}} - \hat{\mathbf{x}}_\mathbf{o})^{\mathbf{T}} \mathbf{B}^{-1} (\hat{\mathbf{x}} - \hat{\mathbf{x}}_\mathbf{o}) \quad (3.8)$$

Retrievals with $\chi^2 > 20$ were rejected, based on the expected distribution of χ^2 for 99 % of a population with 8 degrees of freedom. However, the choice of χ^2 threshold was found not to be critical, as it had a small influence on the statistics of the retrievals.

3.6 Requirements, advantages, and limitations

The described techniques present different requirements, strengths, and limitations. Requirements for M-REG are quite demanding. In fact, apart from sites where simultaneous radiosondes and ground-based radiometric measurements have been routinely performed, it is uncommon to have such an *a priori* dataset available. Conversely, techniques based on simulations (as S-REG, NN, OEM, 1D-VAR) do not need past radiometric measurements, but require *a priori* atmospheric profiles, instrument error characteristics, and an RTE model. For S-REG and NN, the *a priori* set is used for training. However, it is important to ensure the training set covers the expected range of conditions, specially for NN, whose response is unpredictable outside the training range. Differently, OEM and 1D-VAR use a single first guess *a priori* profile and an estimate of its covariance, which can be extracted from the *a priori* set. Methods based on a training require one-time computational efforts to fit the operators, but then provide real-time retrieval. Conversely, methods based on iterative solution may require longer computational time, and research efforts to develop faster models for $\mathbf{F}(\mathbf{x})$ and **K**. The 1D-VAR requires also an NWP output to be used as the first guess.

Among the advantages, M-REG is independent of atmospheric absorption models and it implicitly includes any systematic error in the observations, assuming they are stationary. In this regard, M-REG guarantees the best linear unbiased estimation with respect to radiosondes. This is valuable, although sometimes could result in a limitation because it may hide radiosonde sensor errors. The major drawback is that regression operators are strongly linked to the environment where *a priori* measurements were taken, and any use in other environments will likely result in retrieval biases. Conversely, the advantages of simulated-based techniques (S-REG, NN, OEM, 1D-VAR) are in the flexibility that they offer. In fact, simulated *a priori* dataset can be generated virtually for any site and instrument, using radiosondes or NWP output, and RTE models. On the other hand, an important limitation for these techniques consists in the dependency on the atmospheric absorption model, which cause spectroscopic uncertainties to propagate into the retrievals. In addition, any systematic error in the radiometric measurements is not taken into account, unless it is known and introduced explicitly.

An advantage of iterative and neural techniques (as NN, OEM, 1D-VAR) is to offer better performances for the solution of non-linear problems, particularly important for humidity retrievals. Unlike other methods, OEM and 1D-VAR are physically consistent, which in this context means that the solution is known to reproduce the observation vector used in the retrieval within the measurement accuracy (LÖHNERT et al., 2004). However, there are cases when the solution does not converge. For example, this often happens in 1D-VAR when the forecasted background state is far from the truth, as when the NWP model has mis-timed a frontal ap-

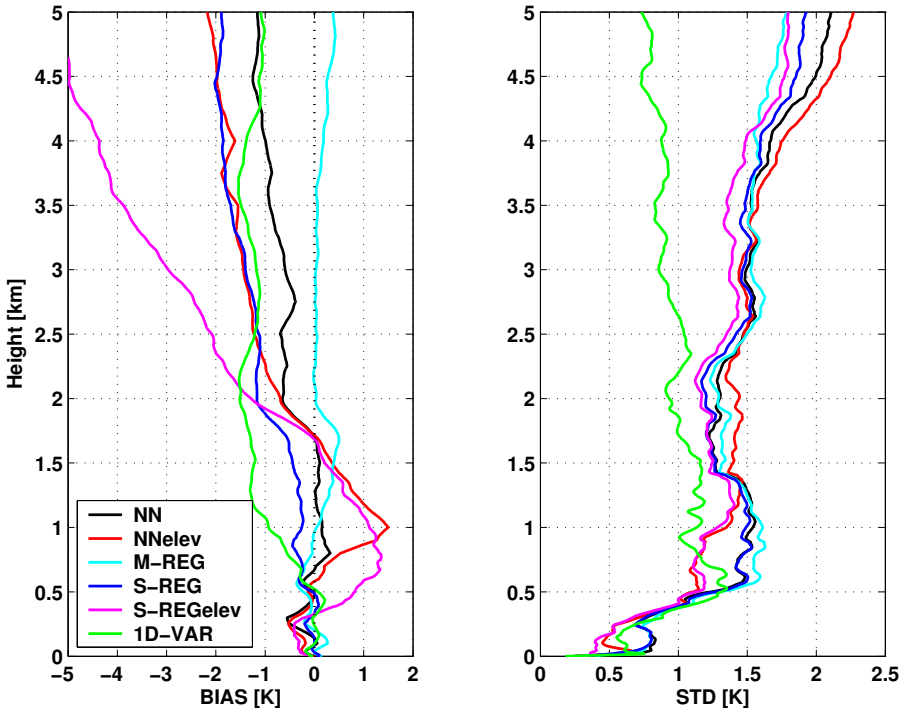

Figure 2: Temperature profile retrieval bias (left) and std (right) with respect to radiosondes (estimate minus *in situ*). All techniques are applied on TP/WVP-3000 measurements.

proach. We recognize that it is difficult for OEM/1D-VAR retrievals to have an impact in these cases, as the assumption of Gaussian errors is no longer valid, and the resulting retrieval is likely to fail quality controls. Besides this, an advantage of 1D-VAR is to initiate the iteration with a background state that is most of the time more representative than a climatological mean, used in other techniques. Moreover, the 1D-VAR can be naturally extended to include other observation with different features. These characteristics make this and similar techniques very appealing for integrated approaches (LÖHNERT et al., 2004).

For the TUC campaign, the S-REG was trained using a 10-year set of winter radiosondes launched in Payerne. The absorption model described in LILJEGREN et al. (2005) was used, adopting the Equivalent Monochromatic Frequency (EMF) estimated by CIMINI et al. (2006) to emulate band-averaged T_b. The NN was trained using the same 10-year set, processed with the LILJEGREN et al. (2005) absorption model at nominal central frequencies. For OEM, $\mathbf{x_o}$ and $\mathbf{B}$ were estimated from monthly means and covariance extracted from a 1-year dataset of radiosondes launched in Payerne. For the parameterisation of $\mathbf{F}$, the forward model described in ROSENKRANZ (1998) was used, while $\mathbf{K}$ was evaluated numerically by small perturbations (Martin et al., 2006b). For M-REG, specific operators had to be computed using radiosonde and radiometric measurements launched during TUC. In fact, due to different environmental conditions, operators based on historical datasets collected at the German Weather Service observatory in Lindenberg (GÜLDNER and SPÄNKUCH, 2001) could not be used in Payerne. In fact, simulation tests showed mean $\mathbf{T}_b$ differences as large as 8 K between the two sites. To leave an independent set for retrieval comparison, the dataset was divided into two parts; only measurements collected during odd-numbered days were used for training of the regression operators.

4 Considerations on expected accuracy

Besides the inversion method, there are other factors determining the retrieval accuracy, defined as the root-mean-square (rms) of estimated minus true profile. For example, in Fig.1 we show simulations of the expected retrieval accuracy difference with respect to a control case (S-REG), when (1) elevation scan observations are used, (2) the number of channels is increased, (3) the synthetic test set is produced with a different absorption model. Negative numbers correspond to a decrease in rms (i.e. better retrieval with respect to the control case).

In exercise (1), we simulated TP/WVP-3000 measurements at the scanning angle in Table 1 and we used this set as input of a variation of S-REG that was trained with observations simulated at the same angles (S-REGelev). As expected (WESTWATER, 1993), Fig.1 shows that the use of elevation scan improves both the temperature and the humidity retrievals in the first kilometre, but has smaller impact at higher levels.

In exercise (2), we simulated a Super Microwave Radiometer (SMWR) to exploit the benefits of integrating the two MWRPs deployed during TUC. Thus, we combined in the SMWR all the 12 TP/WVP-3000 channels, plus 2 (18 and 151 GHz) from ASMUWARA. As shown in Fig.1, the benefits are small, if any, because the 2 channels add little information to the other 12. In the case of ρ profiles, we see a slight decrease in accuracy in the lower 500 m. This is probably due to the fact that linear regression does not handle properly the highly non linear behaviour of 151 GHz T_b. If we limit the test set to dry cases, where the linearity assumption is valid, we expect the 151 GHz channel to contribute positively.

In exercise (3), we generated the training and test sets using two different absorption models (training: LILJEGREN et al., 2005; test: LIEBE et al., 1993). For temperature profiles, the contribution of absorption model uncertainties is rather small (within 0.1 K) in the lower 3 km, although it increase rapidly above that level. This is consistent with the fact that absorption models agree closely in the 55–59 GHz range but diverge in the 51–54 GHz range (HEWISON et al., 2006). For humidity profiles, the retrieval uncertainties in the lower 1.5 km are of the same magnitude of the improvements brought by elevation scan. Thus, improvements in the theoretical knowledge of the spectroscopy seem to be of the same importance, at least, as hardware developments. Therefore, we join other investigators (HEWISON et al., 2006) in encouraging further laboratory studies to reduce absorption model uncertainties in the microwave spectral region.

5 Results during TUC

To assess the quality of the retrievals, the available techniques described in section 3 were applied to the radiometric and surface measurements collected during the TUC campaign. In particular, NN and NNelev are imbedded in the proprietary software associated with the TP/WVP-3000. Additionally, individual customers developed their own software, this being the case for M-REG (DWD, Lindenberg) and 1D-VAR (UK MetOffice, Exeter). The OEM method was implemented by the developers of ASMUWARA for its retrievals (MARTIN et al., 2006a, b), while S-REG and S-REGelev were implemented exclusively for this experiment. Therefore, NN, NNelev, M-REG, S-REG, S-REGelev, and 1D-VAR were applied to TP/WVP-3000 observations, while OEM, S-REG, and S-REGelev to ASMUWARA measurements. A tentative integration of the two instruments (SMWR) was done with S-REG. The most relevant results are illustrated below.

5.1 Method

The retrieved profiles were compared with the set of Meteolabor SRS 400 radiosonde observations launched during TUC. The accuracy of these measurements was investigated using high quality sensors as reference, and estimated to be 0.2 K for temperature and 0.15 g/m^3 for humidity profiles (RUFFIEUX et al., 2006). Both clear- and cloudy-sky periods were used, while rainy cases were screened out using the rain sensor on the TP/WVP-3000. Symmetric views during each elevation scan were averaged in order to reduce the impact of random atmospheric inhomogeneity as well as systematic error on pointing angle. An additional screening, discussed in section 5.5, was necessary to identify cases with highly inhomogeneous sky that influenced the retrievals using elevation observations. When available, retrieved profiles were averaged for the period extending from 5 min before to 25 min after the launch, roughly the time necessary for the balloon to travel the lower troposphere. We reduced the set to be valid as an independent test for all techniques (e.g. cases used in M-REG training were excluded), leaving a sample of 65 radiosondes.

5.2 Temperature profiles

In Figure 2, the temperature retrieval accuracy is evaluated in terms of mean (bias) and standard deviation (std) of the retrieval minus radiosonde profile difference. Only results from TP/WVP-3000 are shown, because ASMUWARA 50–55 GHz channels did not work properly during the experiment. All the techniques based on a synthetic training (NN, NNelev, S-REG, and S-REGelev) show a negative bias between 1.5 and 5 km. This is likely to be related to the 1–2 K inconsistency of the observed and modelled $\mathbf{T}_b$ in the 51–54 GHz channels (HEWISON et al., 2006). This bias was found to be larger in colder/drier conditions. Thus, the bias in temperature profile may be caused by a spectroscopic bias in the absorption models. The two techniques using elevation data (NNelev and S-REGelev) show larger bias than the correspondent techniques using zenith observations only (NN and S-REG). This agrees with the previous considerations, because absorption model uncertainties have larger impact on low elevation angles. Also, NNelev and S-REGelev show about 1 K bias in the retrieved profile between 0.5 and 1.5 km that was not present in NN and S-REG. This could be related to the positive bias at low elevation found in 53.85 GHz (HEWISON et al., 2006), as this frequency is sensitive to lower altitudes. M-REG retrievals show the smallest bias, limited within 0.5 K up to 5 km. This was expected, as the M-REG is not affected by absorption models or instrumental bias, providing the best unbiased linear estimate with respect to radiosondes.

The right panel of Fig. 2 shows the retrieval std, which would indicate the retrieval accuracy in the assumptions of zero-bias and ideal radiosonde measurements. Most of the considered techniques show very little differences, although we can see a slight improve-

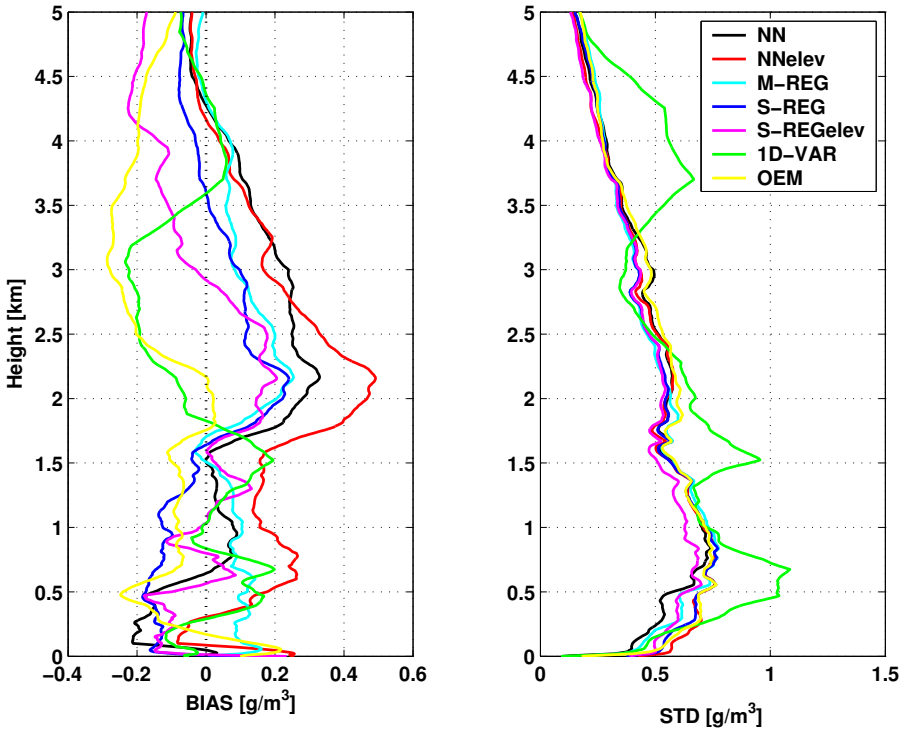

Figure 3: Water vapour profile retrieval bias (left) and std (right) with respect to radiosondes (estimate minus *in situ*). OEM is applied on ASMUWARA measurements; all other techniques are applied on TP/WVP-3000 measurements.

ment related to elevation-based techniques in the lower 1 km. This confirms the theoretical results in Fig.1, although the model-related bias at the same levels would dominate.

Concerning 1D-VAR, the bias is also affected by the absorption model error, although the std improves significantly, especially above 2 km. This is due to the choice of background atmospheric state vector. In fact, 1D-VAR initiates the iteration with a forecast state vector, which is usually more representative of the actual state than the climatologic mean used in other techniques. The improvement is particularly evident above the first kilometre, where the instrument sensitivity starts to fade, and the background state has more impact on the retrieval. Overall, performances for 1D-VAR temperature retrievals from TP/WVP-3000 measurements are similar to those obtained by LILJEGREN et al. (2005) by combining TP/WVP-3000 with satellite-based retrievals.

5.3 Humidity profiles

Similar to Figure 2, Figure 3 shows the accuracy for water vapour density retrievals. Note that we add the OEM retrievals obtained from ASMUWARA data. The bias for NN, S-REG, and M-REG are rather in accordance, especially above 1 km. Even below that, differences are within ± 0.1 g/m^3. Bias from OEM is of the same order, but of opposite sign. As discussed in CIMINI et al. (2006), 22.2 GHz channels in TP/WVP-3000 and ASMUWARA showed about 1.7 K bias during TUC. This, together with the different choice of absorption model, is likely the explanation of the opposite sign.

As predicted by simulations in Figure 1, the observations at different elevation used in S-REGelev bring some improvement with respect to S-REG, especially in the vertical range 0.2–2 km. However, this is not confirmed by the NNelev technique, which actually performs worse than the respective NN. This feature is discussed in more detail in section 5.5.

In contrast to the temperature, for humidity retrievals 1D-VAR is not performing better than other techniques. This might be due to the choice of total water as the humidity component of the state vector. In fact, this choice causes cases with poorly retrieved cloud liquid to dominate the statistics. This may be improved by applying a minimisation technique more appropriate to moderately non-linear problems. It is also hoped that this will improve by the addition of infrared radiometer and/or ceilometer observations. The bias on the humidity retrievals is, however, satisfactory.

5.4 Vertical resolution

Another term to evaluate is the vertical resolution achieved for the retrieved profiles. In fact, the vertical resolution of passive ground-based retrievals of atmospheric profiles depends on many factors, including the spectral and angular information, the consistency of the radiative tranfer, and the quality of the background state vector. Here we adopt the definition proposed by

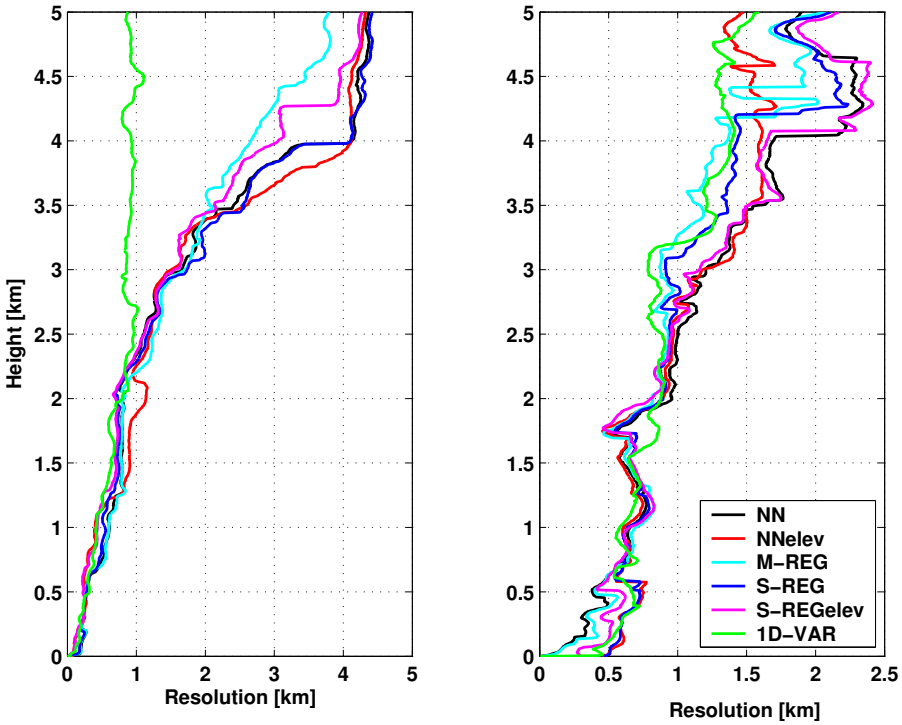

Figure 4: Vertical resolution for temperature (left) and water vapour (right) profile retrievals. All techniques are applied on TP/WVP-3000 measurements.

SMITH et al. (1999), which makes use of the inter-level error covariance. Results obtained applying this method to retrievals from different techniques are shown in Figure 4. For temperature profiles (left panel), the vertical resolution of all methods increases approximately linearly with altitude as half the height from the surface to 3 km. Above this, the resolution of 1D-VAR retrievals continues to increase steadily, while other methods increase more rapidly. Elevation scanning slightly improves the resolution in the boundary layer, but also at some higher levels. Overall, 1D-VAR provides a vertical resolution better than 1 km up to 5 km. Similar results were obtained by LILJEGREN et al. (2005) by combining TP/WVP-3000 with satellite retrievals.

For the humidity profiles (right panel), all techniques show very similar resolution. As for the retrieval std, S-REGelev demonstrates the improvements brought by elevation scanning, showing a slightly better resolution in the lowest kilometer when compared to S-REG. Again, this is not confirmed by NNelev. Especially in the lower levels, where elevation observations should give a positive impact, NNelev shows a resolution significantly worse with respect to NN. In the next section we discuss this issue in more detail.

5.5 Quality control for elevation scan

As anticipated, results in Figures 2–4 were obtained after a screening identifying cases with highly inhomogeneous sky that influenced the retrievals using elevation observations. In fact, the screening based on the rain sensor removes only cases in which precipitation occurs over the instrument. However, clouds and rain located away from the zenith direction create a inhomogeneous scenario that can result in an asymmetry in elevation scan observations. Both NNelev and S-REGelev rely on homogeneous atmospheric stratification and average together the observations taken at two sides in order to reduce the impact of any systematic or random asymmetry. Nevertheless, an inhomogeneous scenario may cause $\mathbf{T}_b$ differences as large as 100 K at symmetric angles, and a simple average may be misleading. This is especially true for NNelev, because of its non-linear characteristics. A way to monitor the atmospheric homogeneity along the direction of scanning is to introduce an equivalent zenith T_b (EZT_b), which corresponds to the $\mathbf{T}_b$ at different elevation angles mapped into opacity (via an estimate of the mean radiating temperature (WESTWATER, 1993)), scaled by the corresponding air mass, and then converted back to T_b. For an ideal homogeneously stratified atmosphere, the standard deviation of EZT_b ($STDEZT_b$) of each scan would be within the radiometer noise level, while in a real scenario this quantity tends to increase for increasing asymmetry. Therefore, a check on the $STDEZT_b$ of each scan is useful to detect asymmetric conditions that may confuse an elevation-based algorithm. As an example, in Figure 5 we show the effect of the $STDEZT_b$ screening applied to both NNelev and S-REGelev. Here we use the $STDEZT_b$ at 30 GHz, this frequency being rather transparent to atmospheric gases but fairly sensitive to liquid water,

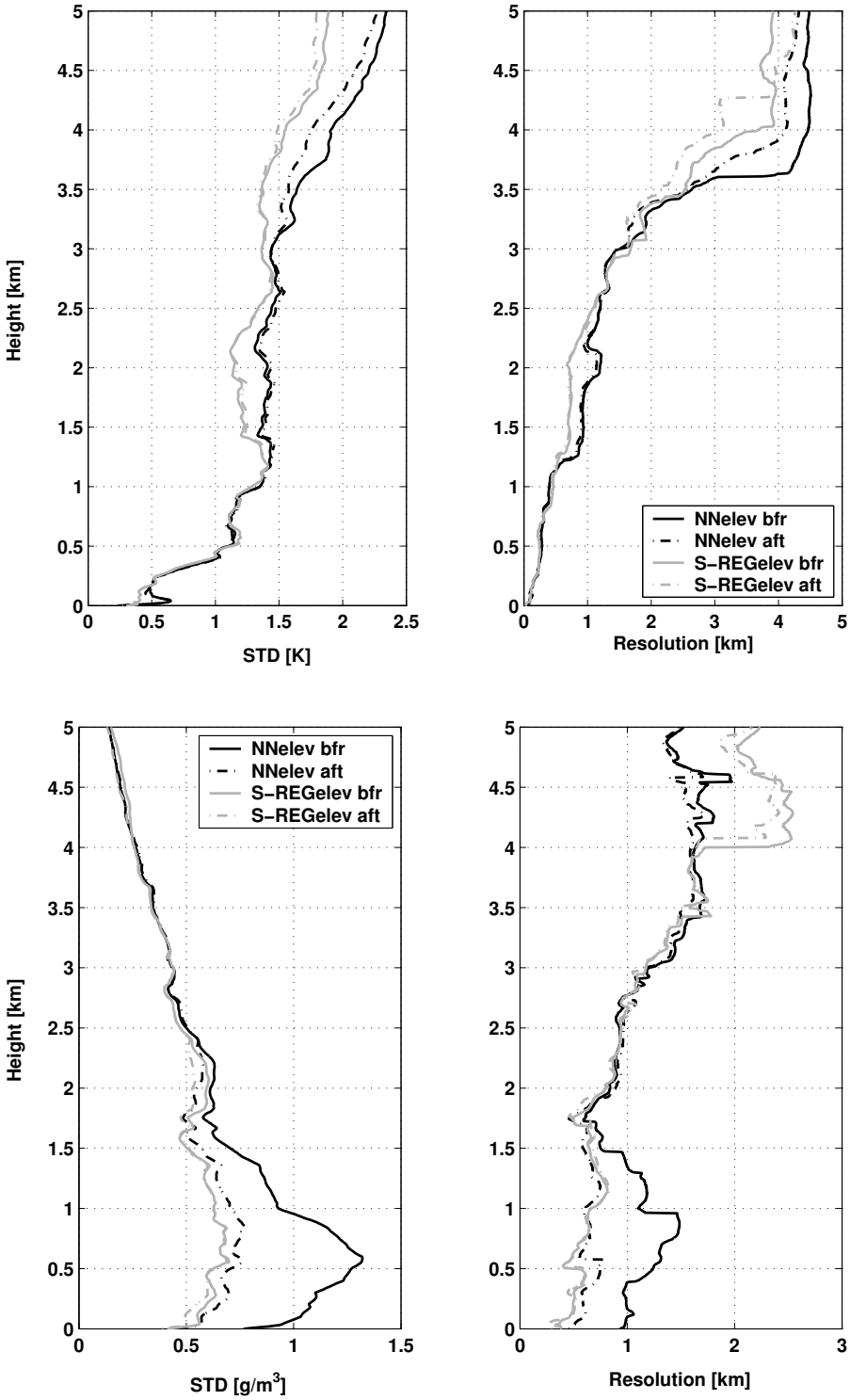

Figure 5: Standard deviation (left) and resolution (right) for NNelev and S-REGelev before and after the STDEZT$_b$ screening. Top panels show temperature retrievals, bottom panels humidity retrievals. Both techniques are applied on TP/WVP-3000 measurements.

with a threshold of 2 K, which represents a loose constraint for clear sky while it is relatively restrictive for cloudy conditions. As evident in Figure 5, the STDEZT$_b$ screening has little impact on the temperature profile retrievals at lower altitude, although both accuracy and resolution slightly improve for higher levels. Information on temperature at these levels is provided by low absorption channels in the oxygen band, which are affected by liquid water emission and hence by cloud/rain inhomogeneities. Conversely, the STDEZT$_b$ screening show large impact on the NNelev humidity profile retrievals. Especially in the lower kilometers, both accuracy and

resolution improve substantially after the screening of highly asymmetric cases. On the other hand, the effect on S-REGelev is much smaller due to its linear response.

Thus, the profiling performances of elevation-based algorithms, in particular non-linear ones such as NNelev, largely depend on the level of atmospheric homogeneity. Therefore, we strongly recommend the use of a quality control for the elevation scan, as for example the one discussed.

6 Discussion and conclusions

This paper describes some of the tools for atmospheric temperature and humidity profiling available during the TUC campaign. Two microwave radiometers and a variety of inversion methods are introduced and characterized. The achieved accuracy of the retrievals is demonstrated in terms of bias, std, and vertical resolution with respect to simultaneous radiosonde observations. The results confirm theoretical expectations that most of the information from ground-based radiometers is concentrated in the lowest 3 km. The temperature and humidity retrieval accuracy is best near the surface and degrades with height to $\sigma_T < 1.5$ K, $\sigma_\rho < 0.7$g/m^3 by 3 km, respectively. Similarly, the vertical resolution degrades linearly with height, z, as approximately 0.44z for temperature and 0.3+0.24z for humidity from 0–3 km. Above 3 km, the retrieval accuracy and resolution degrade rapidly for all techniques, except 1D-VAR, which takes this information from a NWP short range forecast. This highlights the likely impact of these observations in NWP.

In the lowest 1 km, the bias in the temperature and humidity retrievals of most methods is acceptable at $< \pm 0.5$ K and $< \pm 0.2$ g/m^3, respectively. However, at higher levels, most temperature retrievals showed a negative bias of 1–2 K, which was found to be larger in colder/drier conditions. This is likely to be related to difference found between modelled and observed T_b in the 51–54 GHz channels (HEWISON et al., 2006), which may arise from spectroscopic errors in the absorption models. This is supported by the fact that the technique which does not rely on absorption models does not show the same bias.

Elevation scanning is expected to improve the accuracy and resolution of retrieved profiles in the boundary layer. Although we show some improvements, these are limited by atmospheric inhomogeneity, absorption model uncertainty, and mechanical limitations. For example, elevation scanning improves the std of a regressive method, but increases its bias. Furthermore, a quality control of the atmospheric homogeneity seems to be crucial for a non-linear approach, and thus it is strongly recommended.

Optimal Estimation methods, such as 1D-VAR, offer a convenient way to combine observations from microwave radiometers with a background (e.g. from NWP) accounting for their error characteristics. This also allows integration of data from other instruments as described by LÖHNERT et al. (2004). Currently the humidity retrievals are dominated by poorly retrieved liquid water, but may be improved using a non-linear minimization. We plan to extend this method to include infrared radiometer observations and refractive index gradients derived from collocated wind profiling radar (KLAUS et al., 2006). It is hoped that this will improve the accuracy and vertical resolution of the humidity retrievals.

Acknowledgements

The work presented in this paper was sponsored by the COST-720 project. D. CIMINI's contribution was prepared during his period at CETEMPS, University of L'Aquila, CIRES, University of Colorado, and IMAA, National Research Council. All three institutions are kindly acknowledged.

References

CIMINI, D., T. J. HEWISON, L. MARTIN, 2006: Comparison of brightness temperatures observed from ground-based microwave radiometers during TUC. – Meteorol. Z. **15**, 19–25.

DEBLONDE, G., S.J. ENGLISH, 2003: One-Dimensional Variational Retrievals From SSMIS Simulated Observations. – J. Appl. Meteor. **42**, 1406–1420.

GÜLDNER, J., D. SPÄNKUCH, 2001: Remote sensing of the thermodynamic state of the atmospheric boundary layer by ground-based microwave radiometry. – J. Atmos. Oceanic Technol. **18**, 925–933.

HEWISON T. J., D. CIMINI, L. MARTIN, C. GAFFARD, J. NASH, 2006: Validating atmospheric absorption models in clear air using ground-based microwave radiometers. – Meteorol. Z. **15**, 27–36.

JANSSEN, M. A., 1993: An introduction to the passive microwave remote sensing of atmospheres. In: JANSSEN, M. (Ed.): Atmospheric Remote Sensing by Microwave Radiometry, New York, Wiley.

KLAUS, V., L. BIANCO, C. GAFFARD, M. MATABUENA, T. J. HEWISON, 2006: Combining Radar Wind Profiler and Microwave radiometer for the estimation of atmospheric humidity profiles,. – Meteorol. Z. **15**, 87–97.

LIEBE, H.J., G.A. HUFFORD, M.G. COTTON, 1993: Propagation Modeling of Moist Air and Suspended Water/Ice Particles at Frequencies Below 1000 GHz. – AGARD 52nd Specialists' Meeting of the Electromagnetic Wave Propagation Panel, Ch3.

LILJEGREN, J.C., S.A. BOUKABARA, K. CADY-PEREIRA, S.A. CLOUGH, 2005: The Effect of the Half-Width of the 22-Ghz Water Vapor Line on Retrievals of Temperature and Water Vapor Profiles with a Twelve-channel Microwave Radiometer. – IEEE Trans. Geosc. Rem. Sens. **43**, 1102–1108.

LÖHNERT, U., S. CREWELL, C. SIMMER, 2004: An Integrated Approach toward Retrieving Physically Consistent Profiles of Temperature, Humidity, and Cloud Liquid Water. – J. Appl. Meteor. **43**, 1295–1307.

MARTIN L., M. SCHNEEBELI, C. MÄTZLER, 2006a: ASMUWARA, a ground-based radiometer system for tropospheric monitoring. – Meteorol. Z. **15**, 11–17.

—, —, —, 2006b: Tropospheric water and temperature retrieval for ASMUWARA. – Meteorol. Z. **15**, 37–44.

RODGERS, C. D., 2000: Inverse Methods for Atmospheric Sounding: Theory and Practice. – Series on Atmospheric, Oceanic and Planetary Physics, Vol. 2, World Scientific Publishing, Singapore.

ROSENKRANZ, P.W., 1998: Water Vapor Microwave Continuum Absorption: A Comparison of Measurements and Models. – Radio Sci. **33**, 919–928.

RUFFIEUX, D., J. NASH, P. JEANNET, J.L. AGNEW, 2006: The COST 720 temperature, humidity, and cloud profiling campaign: TUC. – Meteorol. Z. **15**, 5–10.

SMITH, W.L., W.F. FELTZ, R.O. KNUTESON, H.E. REVERCOMB, H.M.WOOLF, H.B. HOWELL, 1999: The retrieval of planetary boundary layer structure using ground-based infrared spectral radiance measurements. – J. Atmos. Oceanic Technol. **16**, 323–333.

SOLHEIM, F., J. GODWIN, E. WESTWATER, Y. HAN, S. KEIHM, K. MARSH, R. WARE, 1998: Radiometric Profiling of Temperature, Water Vapor, and Cloud Liquid Water using Various Inversion Methods. – Radio Sci. **33**, 393–404.

WARE, R., F. SOLHEIM, R. CARPENTER, J. GUELDNER, J. LILJEGREN, T. NEHRKORN, F. VANDENBERGHE, 2003: A multi-channel radiometric profiler of temperature, humidity and cloud liquid. – Radio Sci. **38**, 8079, doi:10.1029/2002RS002856.

WESTWATER, E., 1993: Ground-based Microwave Remote Sensing of Meteorological Variables. – In: JANSEN, M. (Ed.): Atmospheric Remote Sensing by Microwave Radiometry, Wiley & Sons, Inc., 145–213.